Ceramics International 49 (2023) 22149–22159

Contents lists available at ScienceDirect

Ceramics International

journal homepage: www.elsevier.com/locate/ceramint

Phosphate-based geopolymer: Influence of municipal solid waste fly ash introduction on structure and compressive strength

Davide Bernasconi [a,*], Alberto Viani [b], Lucie Zárybnická [b], Petra Mácová [b], Simone Bordignon [c], Caterina Caviglia [a], Enrico Destefanis [a], Roberto Gobetto [c], Alessandro Pavese [a]

[a] Earth Sciences Department, University of Turin, Turin, 10125, Italy
[b] Institute of Theoretical and Applied Mechanics of the Czech Academy of Sciences, Centre Telč, Prosecká 809/76, Praha 9, 190 00, Czech Republic
[c] Chemistry Department, University of Turin, Turin, 10125, Italy

ARTICLE INFO

Handling Editor: Dr P. Vincenzini

Keywords:
Phosphate geopolymers
Municipal solid waste fly ash
Metakaolin
Phosphate cement

ABSTRACT

Materials resulting from incorporation of solid waste incineration fly ash into phosphate-based geopolymers, to partially replace metakaolin (up to 50% wt), were studied. X-ray diffraction, scanning electron microscopy, solid-state nuclear magnetic resonance spectroscopy and infrared spectroscopy were adopted to describe the mineralogical changes and the structural modifications of the geopolymer networks which impacted on the mechanical performance (compressive strength) of the materials. The results indicated that fly ash displays a different reactivity compared with metakaolin, behaving preferentially as a source of alkali that compete with the aluminosilicate metakaolin fraction by precipitating crystalline and amorphous phosphates. At 10 wt% of metakaolin substitution with fly ash, the extent and reticulation of the amorphous geopolymer matrix is preserved, and the mechanical properties are retained. At higher waste content (30–50% wt), the fast kinetics of the acid-base reactions involving the fly ash reactive phases prevail over the metakaolin dealumination, and the nature of the material shifts to an alkali-phosphate cement/phosphate-geopolymer composite. This behaviour, together with the development of porosity and presence of low-strength phases in the ash, led to a decline in the mechanical performance with increasing amount of substitution. All in all, this work provides fundamental information in the direction of a sustainable employment of phosphate-based geopolymers, which is limited by the relatively high cost of both metakaolin and phosphoric acid. Moreover, it indicates a recycling opportunity for this type of fly ash.

1. Introduction

The ever-increasing necessity to reduce the environmental footprint of the large-scale high temperature manufacturing has prompted potentially more sustainable alternatives, in terms of primary/secondary raw materials and processes, paying special attention to the building and ceramics materials [1–4]. In this scenario, the interest for geopolymers has steadily grown [5–7], though much work is still required to overcome difficulties such as compression of the production costs, definition of the curing method and improvement of technical performances. Geopolymers represent an amorphous ceramic-like class of materials usually obtained by reacting an aluminosilicate "source" with a strong alkali base at room temperature, so as to generate a highly reticulated matrix of poly(siloxo)/poly(sialate) (Si-O-Si-O-/Si-O-Al-O-) units [8,9]. The resulting product exhibits high mechanical performance and fire resistance [7–9]. Initially, metakaolin (MK), from the calcination of natural kaolinite at temperatures >700 °C, was chosen as an aluminosilicate source because of its reactivity related to a large amorphous fraction and fine particle size. However, environmental and economic concerns due to both high temperatures needed for its production and exploitation of natural resources for provision of kaolinite, are motivating efforts steered to an at least partial replacement of MK [7,9]. Ground blast furnace slag (GBFS) [10], coal fly ash (CFA) [11], mine tailings [12] and also municipal solid waste incineration fly ash (MSWI-FA) [13,14] have been/are being tested, alone or in blends, to reduce the amount of required MK and provide a recycling opportunity for these solid waste residues thereby.

Another viable route for geopolymers preparation involves the use of an acid solution, like phosphoric acid (H_3PO_4), to dissolve/depolymerize the network of a raw material and produce a new polymeric

* Corresponding author.
E-mail address: davide.bernasconi@unito.it (D. Bernasconi).

https://doi.org/10.1016/j.ceramint.2023.04.042
Received 20 January 2023; Received in revised form 20 March 2023; Accepted 7 April 2023
Available online 7 April 2023

structure formed by polysilicoalumino-phospho (-Al-O-P-O-Si-) units [7,15]. This system, which can be defined as a *phosphate-based geopolymer* (PBG), has hitherto received less attention than the alkali-based analogues, although it performs better in terms of thermal stability and resistance to corrosion and efflorescence [7,16]. Moreover, PBG provides a promising matrix to incorporate and functionalise waste residues, thus contributing to reduce its production costs and promote sustainability-policy at large. Few studies have to date investigated the implementation of solid waste residues in PBG, and they mostly focused on CFA. In particular, Guo et al. [17] show that a substitution of MK with CFA up to 30 wt% provides a material exhibiting good mechanical properties. In addition, Wang et al. [18] tested both low- and high-calcium CFA, concluding that the former acts as a secondary aluminosilicate precursor while the latter behaves as a rapid consolidation agent (hereafter, "setting agent"), through calcium phosphate phases precipitation.

In the present work, we explore the replacement of MK with previously water/steam-washed MSWI-FA [19,20], in phosphate-based-geopolymers, in order to make such a class of geopolymers as sustainable as possible in terms of economic and environmental costs. In particular, we aim to understanding how the MSWI-FA/MK-PBG interaction affects the PBG molecular framework, which in turn is related to the mechanical performance that underlies the potential marketability of an item produced by such a material. MSWI-FA represents one of the solid by-products that are produced during the municipal solid waste incineration process. It is collected from the flue gases purification system, and it usually accounts for about 3–15% of the total incinerated waste volume [21]. MSWI-FA is composed of irregularly shaped micron-scale fine particles (commonly, more than 90% of the particles are below 150 μm in size), and bears a relatively high content of chloride, sulphate salts and heavy metals (i.e., Zn, Pb, Cd, Cr, Ni) [22]. Many efforts have been devoted to the development of suitable treatment strategies to handle its disposal and, in the recent years, special attention has been paid to recycling technologies, which add an economic value to such a residue and realize a sustainable alternative to landfilling. MSWI-FA, owing to its chemical composition (rich in Ca, Si, Mg, Al and Fe) and small particle size (commonly, more than 90% of the particles are below 150 μm in size), can be of interest in manufacturing and civil engineering applications, provided that it is pre-treated, usually by water washing [20–22]. The resulting residue has been widely tested as a supplementary cementitious material to partially replace raw materials in ordinary Portland cement (OPC) and low-energy cements, such as alinite and calcium sulfoaluminate cements [23–27]. In the PBG context, the metal ions provided by the MSWI-FA may be involved in reactions with phosphoric acid to form metal phosphates, similarly to what happens in the preparation of the acid-base chemically bonded ceramics [28,29].

Composition and microstructure of the obtained geopolymer samples were characterized by Fourier-transform infrared spectroscopy (FT-IR), solid-state nuclear magnetic resonance (SS-NMR), X-ray powder diffraction (XRPD), scanning electron microscopy (SEM-EDS) and mercury intrusion porosimetry (MIP). Eventually, the mechanical performance of the obtained materials was assessed through compressive strength tests. To our knowledge, incorporation of MSWI-FA into acid geopolymer matrixes is a subject little investigated, and the present work was designed to be a contribution to fill such a gap.

2. Experimental

2.1. Materials

Industrial metakaolin was obtained from České lupkové závody, a.s. (Czech Republic) and produced by heating kaolinite at 750 °C for 2 h. Reagent grade phosphoric acid solution (85% wt) was bought from Lach-ner s.r.o (Czech Republic). MSWI-FA from a waste-to-energy plant in Turin (Italy) was fully characterised in an earlier investigation [30]. Before being used, MSWI-FA underwent a water/steam washing treatment [19,20] (liquid-to-solid ratio of 10, time of treatment of 24 h; steam flux of 2 L/min, humidity of 40% v/v, time of treatment of 10 min), to reduce the content of the soluble phases and curb the related heavy metal leaching thereby. The washed fly ash was filtered and then milled in a steel ball mortar (RM 200, Retsch, Germany) to a particle size <63 μm. The BET surface area, mean particle size, chemical composition (X-Ray Fluorescence measurements) and mineralogical composition (X-ray powder diffraction and Rietveld method) of the used primary/-secondary raw materials are presented in Tables 1 and 2. The results reported therein are the average of 3 repetitions on different samples.

2.2. Geopolymer formulation

Table 3 reports details about the formulation of the investigated MSWI-FA geopolymer pastes. They were obtained by addition of a proper amount of diluted phosphoric acid solution into different blends of MK and MSWI-FA, which were previously hand-mixed to ensure homogeneity. The acid solutions were obtained by dilution of reagent grade phosphoric acid (85% wt; 14.7 M) in ultrapure water and then stored for 24 h prior to use. The resulting slurry was stirred manually for 5 min and then cast into cubic polytetrafluoroethylene (PTFE) molds ($10 \times 10 \times 10$ mm^3), which were kept on vibration for 1 min to remove possible air bubbles. The molds were successively wrapped in plastic foils to prevent evaporation and subjected to a two-step curing treatment, consisting of 24 h at room temperature and 24 h at 60 °C. Such a curing method was chosen because of its proven efficacy to reduce cracks in the resulting material [31]. Eventually, the geopolymer samples were aged at room temperature, for as long as 60 days. We chose an Al/P nominal molar ratio of 1.1, as such a figure allows a satisfactory workability of the paste according to preliminary tests. The samples of the present study are univocally identified by the label "PBGX", where "X" is the wt% of MSWI-FA in replacing MK.

2.3. Analytical methods

The phase composition was determined by XRPD measurements using a Miniflex 600 diffractometer (Rigaku, Japan), with Cu-Kα incident radiation and operated at 40 kV–15 mA. XRPD patterns were collected between 5° and 60° 2θ, with a 2θ-step size of 0.02 and scan speed of 0.1°/min. The Rietveld analysis, using high purity ZnO as an internal standard (10 wt%), was employed to determine the mineralogical composition of the raw materials. Data refinements were carried out by the software Topas 4.6.

FTIR-ATR spectra were collected on a Fourier transform Equinox 55 (Bruker) spectrophotometer equipped with an ATR device; the resolution was set at 2 cm^{-1} for all spectra. A spectral range of 600–4000 cm^{-1} was scanned, using KBr as a beam splitter.

All SS-NMR measurements were recorded at room temperature on a solid-state NMR spectrometer (JNM-ECZ600R, JEOL RESONANCE Inc., Japan) with a magnetic field of 14.1 T, operating at ^{27}Al, ^{29}Si, and ^{31}P Larmor frequencies of 156.4, 119.2, and 242.9 MHz, respectively. The samples were packed into 3.2 mm zirconia rotors and spun at a MAS frequency of 15, 15 and 20 kHz for ^{27}Al, ^{29}Si, and ^{31}P MAS spectra, respectively. A^{27}Al, ^{29}Si and ^{31}P pulse of 12 μs, 4 μs and 3 μs were employed, with relaxation times of 10, 10 and 20 s ^{27}Al, ^{29}Si, and ^{31}P chemical shifts scales were referenced through the resonances of aluminium nitrate, silica and $(NH_4)H_2PO_4$, respectively. The deconvolution analysis was carried out using the related in-built feature of Delta 6.1 (Jeol), while the estimated uncertainty on the determined fractions is in range of ±1%.

Secondary electron (SE) and back scattered electron (BSE) images were collected, and chemical composition analyses were performed by a Scanning Electron Microscope JSM IT300LV High Vacuum – Low Vacuum 10/650 Pa – 0.3–30 kV (JEOL USA Inc.), operating at the following conditions: W filament, EHT 15 kV, standard probe current and working

Table 1
Chemical composition (wt %) and main physical properties of MK and MSWI-FA. Uncertainties of about 2–3%.

Raw materials	Chemical composition (wt %)												
	Al_2O_3	Fe_2O_3	TiO_2	K_2O	CaO	SiO_2	MgO	SO_3	P_2O_5	Others	BET (m^2g^{-1})	D_{50} (μm)	D_{90} (μm)
MK	42.70	1.09	1.80	0.83	0.58	52.45	0.18	0.07	0.08	0.14	12.8	3.0	10.0
MSWI-FA	7.37	8.99	2.87	0.45	44.38	22.51	6.98	5.23	0.38	0.86	15.7	8.8	29.1

Table 2
Mineralogical composition (wt %) of MK and MSWI-FA, using the Rietveld analysis on X-ray powder diffraction patterns. The uncertainties are ±0.5 wt % (crystal phases) and ±5 wt % (amorphous phase).

	MK	MSWI-FA
Quartz	3.9	4.3
Kaolinite	2.2	
Anatase	1.1	
Illite	1.2	
Mullite	1.6	
Calcite		7.5
Anhydrite		9.6
Larnite		3.0
Gehlenite		6.2
Periclase		4.0
Gypsum		4.5
Bassanite		1.1
Ettringite		3.8
Merwinite		1.7
Perovskite		2.3
Amorphous	90	52

Table 3
Formulations of MK/MSWI-FA geopolymer pastes. The Al/P mole ratio was determined on the basis of the chemical composition of MSWI-FA and MK, and of their proportion in the solid mixtures. The molar ratio of Al/P was kept to 1.1 by adjusting the mass of phosphoric acid. L/S: mass ratio between the diluted phosphoric acid solution (L) and the mass of the used raw materials (S). M: molarity of the diluted phosphoric acid solution.

Sample	Solid binder		Al/P	L/S	M(mol L^{-1})
	MK (wt %)	MSWI-FA (wt %)			
PBG0	100	0	1.1	0.90	12
PBG10	90	10	1.1	0.90	12
PBG20	80	20	1.1	0.93	10
PBG30	70	30	1.1	0.95	9
PBG50	50	50	1.1	1.00	6

distance 7 mm for images and high probe current and working distance 10 mm for chemical analysis.

PBG's final setting time was measured using a Vicat needle on samples which did not undergo any thermal curing treatment. The test was considered completed when the needle failed to penetrate more than 0.5 mm into a sample. The experiments were carried out in triplicate (3 replicates for each formulation have been tested) and the average values were reported.

Compressive strength tests were performed on early (7 days) and long-aging (60 days) PBG cubes (1x1x1 cm), measuring 5 replicates by means of an Instron 3345 (Instron, USA) loading frame, at loading speed of 0.2 mm/min and load cell of 5 kN.

Porosity was determined by mercury intrusion technique on long-aging (60 days) PBG paste cubes (1x1x1 cm), using a Mercury porosimeter (Autopore IV 9500, Micromeritics Corporation, USA).

3. Results

3.1. X-ray powder diffraction (XRPD)

The PBG0 pattern (Fig. 1) is characterized by an evident amorphous "hump" centred at around 2θ-25°, in agreement with the amorphous components in the system [32]. The residual minerals in MK (Table 2) are still observable in all of the PBG-samples. The introduction of

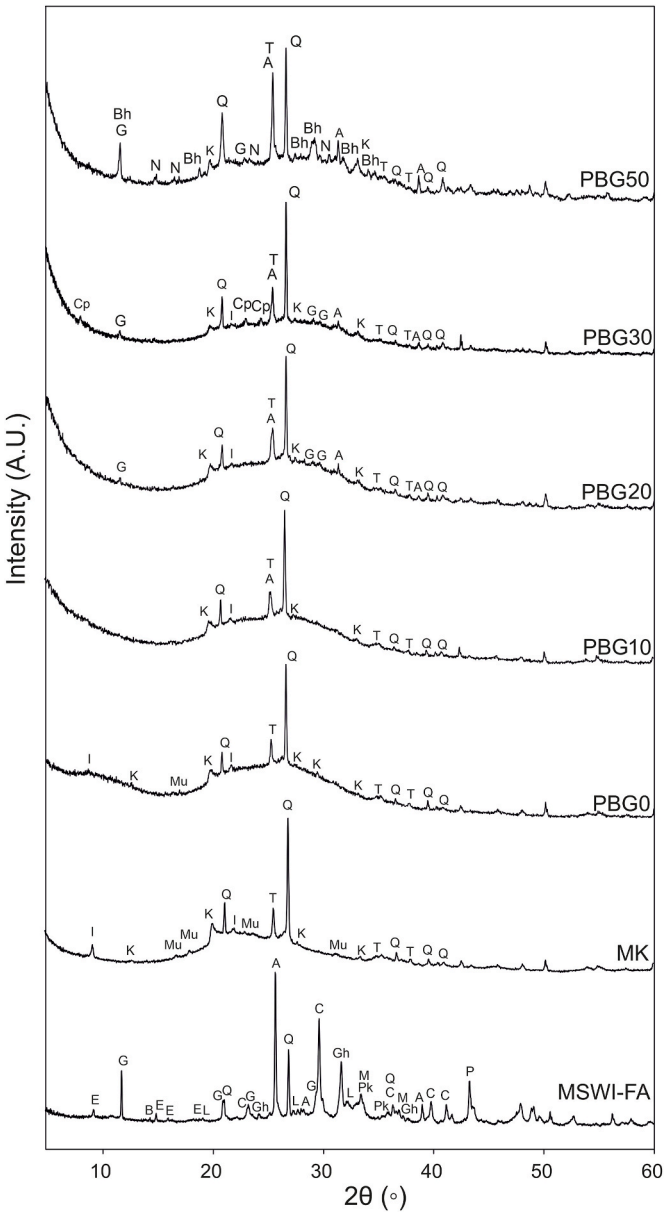

Fig. 1. XRPD patterns of metakaolin, MSWI-FA and PBG0-10-20-30-50 samples, cured for 60 days. The symbols are as follows; A (Anhydrite, $CaSO_4$); B (Bassanite, $CaSO_4{\cdot}0.5H_2O$); Bh (Brushite, $CaHPO_4{\cdot}2H_2O$); C (Calcite, $CaCO_3$); Cp (Monocalcium phosphate hydrate, $Ca(H_2PO_4)_2{\cdot}H_2O$); E (Ettringite, $Ca_6Al_2(SO_4)_3(OH)_{12}{\cdot}26H_2O$); G (Gypsum, $CaSO_4{\cdot}2H_2O$); Gh (Gehlenite, $Ca_2Al(AlSi)O_7$); I (Illite, $KAl_2Si_4O_{10}(OH)_2$); K (Kaolinite, $Al_2Si_2O_5(OH)_4$); L (Larnite, Ca_2SiO_4); M (Merwinite, $Ca_3Mg(SiO_4)_2$); Mu (Mullite, $Al_6Si_2O_{13}$); N (Newberyite, $MgHPO_4{\cdot}3H_2O$)P (Pericalse, MgO); Pv (Perovskite, $CaTiO_3$); Q (Quartz, SiO_2); T (Anatase, TiO_2).

MSWI-FA, up to a replacement of MK in terms of 20 wt%, exhibits a comparatively modest effect on the crystalline fraction of PBGX. The MSWI-FA's phases, which likely react in the acidic phosphate environment, are calcite, ettringite and periclase [28,33]; the secondary products that form in PBGX (likely Ca and Mg phosphates) are either non-crystalline, similarly to what observed in the Mg- or Ca-Mg phosphate cements [28,34], or in a too low abundance to allow detection. With the introduction of larger fractions of MSWI-FA (PBG30 and PBG50), new crystalline phosphates appear: in PBG30, monocalcium phosphate monohydrate [MCPM, $Ca(H_2PO_4)_2{\cdot}H_2O$]; in PBG50, brushite ($CaHPO_4{*}2H_2O$) and newberyite ($MgHPO_4{\cdot}H_2O$). As to the effect on the PBG-structure, due to the amorphous nature of some of the products, the analysis should be conducted from a qualitative standpoint. In previous works, the XRPD background profile was considered to evidence the presence of different coexisting frameworks (amorphous silica and aluminophosphate) [9,35]. In the XRPD patterns of our samples, a reduction of the main amorphous "humps" around 2θ-24° and 2θ-12° with the increase of the MSWI-FA content, is apparent. This suggests a reduced amount of geopolymer matrix, in combination with a shift from a pure PBG-system to a Ca(Mg)-phosphate cement (CMPC)/PBG composite. Further confirmation is obtained from the results of spectroscopic measurements, as reported below.

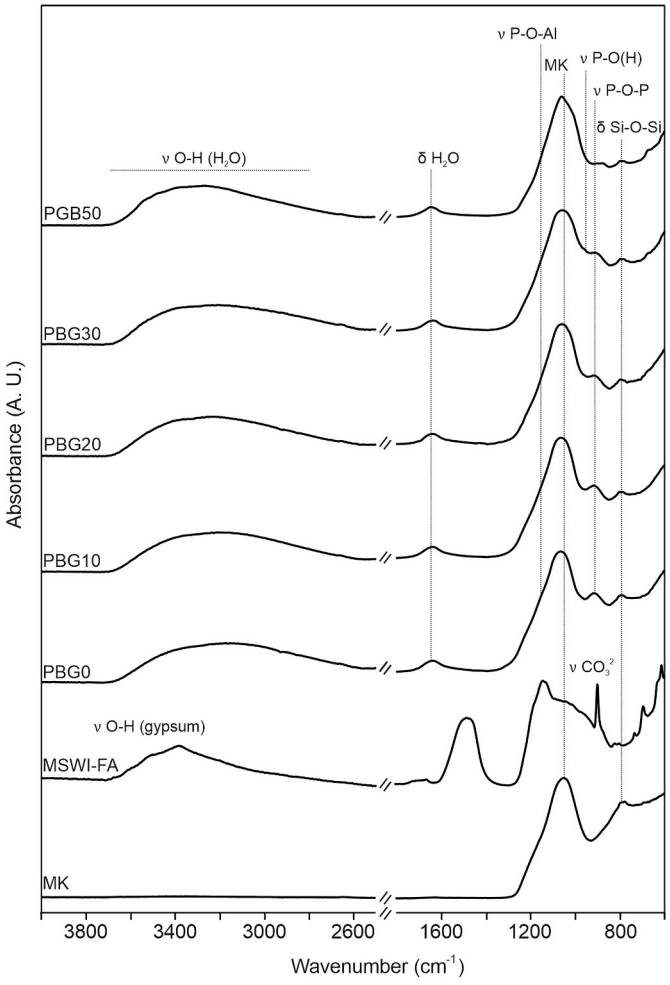

Fig. 2. Infrared spectra of metakaolin, MSWI-FA and PBG0-10-20-30-50 samples cured for 60 day, with the indication of the main assignments. The MK peak maximum is highlighted to visually help recognizing the shift in the PBG samples.

3.2. Infrared spectroscopy

Fig. 2 displays the FT-IR spectra of MK, MSWI-FA and PBG-samples. The infrared spectrum of the raw materials is characterized by a main feature at 1056 cm^{-1}, related to the Si-O-Al stretching vibrations of the aluminosilicate amorphous fraction, along with a doublet around 790-770 cm^{-1} of the residual quartz [35]. In case of MSWI-FA, the broad peak between 1200 and 1000 cm^{-1} encompasses contributions from all the different Si-O and Al-O stretching vibrations of the crystalline and amorphous aluminosilicates. Particularly evident are also the peaks related to calcite, i.e., $\nu_{2,asym}$ and $\nu_{3,asym}$ CO_3^{2-} bands at 1400 and 870 cm^{-1}, respectively [36], along with the ν_{sym} O-H doublet between 3500 and 3400 cm^{-1} of the hydrous phases, like gypsum [37].

The FT-IR spectrum of PBG0 preserves many of the pure MK's features. Yet, some differences are worth being stressed: although the discrimination between ν(Si-O), ν(Al-O) and ν(P-O) is complex, owing to their overlap in the spectral region 1200-1000 cm^{-1} [9,27], a blueshift to 1065 cm^{-1} of the main band occurs. This suggests a rearrangement of the Si-O, Al-O and P-O bonds due to the geopolymerization reactions [38]. In addition, two new bands at 1146 and 908 cm^{-1} can be assigned to ν_{asym} P-O-Al and ν_{asym} P-O-P, respectively [35], thus confirming the presence of a reticulated aluminophosphate framework.

The same features are preserved in the spectra of the samples PBG10 and PBG20, although the vibrations at 1146 and 908 cm^{-1}, associated with the geopolymer structure, seem to have a relatively lower intensity. This suggests that the lower aluminium content of MSWI-FA with respect to MK's negatively affects the development of the aluminophosphate matrix. The main peak blueshift, i.e. 1060 cm^{-1}, is less marked in PBG30 than PBG0-10-20, indicating a reduced rearrangement of the Si-O and Al-O bonds, which remain similar to MK's, thus pointing to a more limited reactivity of the raw materials' mixture. In addition, a new peak at 970 cm^{-1} hints at the presence of the crystalline phosphate phase $Ca(H_2PO_4)_2{\cdot}H_2O$ [39].

3.3. Solid-state nuclear magnetic resonance (SS-NMR)

The SS-NMR is a powerful tool in the structural characterization of geopolymers, due to its capacity to selectively probe specific elements (nuclei) regardless of the occurrence of a long-range order [40]. All the main species involved in the geopolymerization process were investigated: ^{27}Al, ^{31}P and ^{29}Si.

^{27}Al MAS spectra of the raw materials are described in the Supplementary Materials (SM), Fig. S1, while the PBG-samples' spectra are shown in Fig. 3 (left). The PBG0 spectrum is dominated by a peak at about −12 ppm, assigned to octahedral [AlO_6] units linked to tetrahedra [PO_4]. Al^{VI} represents the main aluminium coordination in condensed aluminophosphate geopolymers, at variance with traditional basic geopolymers, wherein Al^{IV} dominates [9,41]. The Al^{IV} signal characteristic of MK is slighlty visible at about 60 ppm, indicating that the dealumination of the raw material was almost complete. The spectrum profiles from MSWI-FA-bearing PBG samples exhibit peaks whose positions are similar to those in PBG0, though they differ in terms of intensity, thus indicating that MSWI-FA affects the degree of geopolymerization.

In a similar way, differences are visible in the ^{31}P MAS spectra (Fig. 3, middle). The reference sample PBG0 displays a single and broad peak between −5 and −20 ppm, characteristic of amorphous condensed phosphate units [40]. Upon increasing the MSWI-FA content, the peak maximum shifts towards a lower field and the peak asymmetry decreases. In PBG30 and PBG50, new and sharper resonances appear; they are consistent with MCPM (−0.1 and −4.5 ppm) [34], in the first case, and with brushite (1.1 ppm) [34] and newberyite (−7.4 ppm) [42], in the second case. An additional peak at about −1.6 ppm is visible in the PBG50 ^{31}P MAS spectrum, close to the reference value of −1.5 ppm for monetite ($CaHPO_4$) [42], though the latter phase has never been detected by X-ray diffraction in our samples.

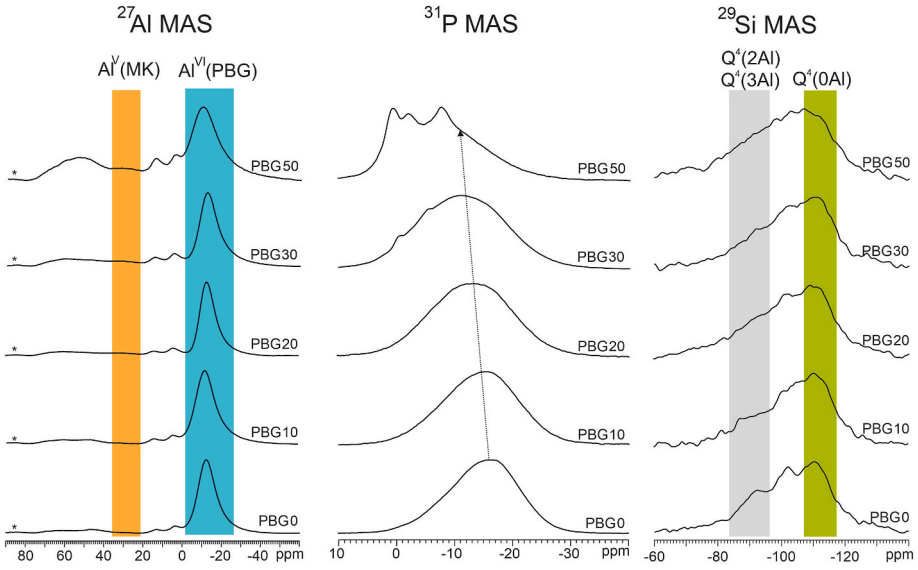

Fig. 3. ^{27}Al MAS (left), ^{31}P MAS (middle) and ^{29}Si MAS (right) spectra of PBG samples cured for 60 days.

Fig. 3 shows the ^{29}Si MAS spectra of the PBG-samples, while in Fig. S2 of SM the spectra from the raw materials are described. The acidic dissolution of MK leads to the release of Al^{3+} and depolymerization of the Si-O layers [15,18,38]; whereas phosphate anions are energetically favoured to make bonds with aluminium to build up the geopolymer structure [9], the residual [SiO_4] are supposed to rearrange into an amorphous silica phase, leading to a composite-like system [9]. In MK, the Si speciation is represented by Q^4_{Si}(mAl), i.e. Si-tetrahedron with four bridging oxygens and m-Al atoms in the second coordination sphere [40]. Once geopolymerization has occurred, in PBG0 prevails a Q^4_{Si}(0Al) component at −112 ppm, associated with a highly reticulated amorphous silica phase. Please, note that the MK dissolution implies a decrease of abundance of the speciation related to Q^4_{Si}(3Al) and Q^4_{Si}(2Al), whose signals lie in the range 85–95 ppm [9]. Upon increasing the MSWI-FA content, the spectra become less and less resolved.

Spectral deconvolutions helped us interpret the role of MSWI-FA in affecting the PBG-structure. The assignments are shown in Figs. S3–S5 of SM. The analysis of the ^{27}Al MAS spectra indicates a secondary contribution due to the [AlO_4] units in PBG-samples at around 45 ppm [38,43]. The contributions of the Al^{VI} and Al^{IV} speciations in the PBG-samples are shown in Fig. 4, with respect to the unreacted Al^{V} of MK. This aluminium coordination in MK is related to the most instable Al fraction in the geopolimerization process [9], and therefore it was chosen as a marker of the raw material reaction degree. The MK Al^{V} peak is absent in PBG0 and PBG10; at a higher degree of substitution, this contribution becomes progressively more and more relevant, while the aluminophosphate fraction decreases concomitantly.

The broad ^{31}P peak was modelled with three contributions, centred at −7, −12 and −17 ppm, which are assigned to the Q^1_P(0Al), Q^1_P(1Al), Q^1_P(2Al) units, respectively [40,43], where Q^n_P(mAl) indicates [PO_4] units bridged with n P-tetrahedra and m Al-polyhedra. In Fig. 4, the most important contribution in PBG0 is from the Q^1_P(2Al) unit, confirming the presence of a highly cross-linked aluminophosphate matrix [38,43]. In PBG10 and PBG20, the Q^1_P(2Al) content decreases in favour of Q^1_P(0Al) and Q^1_P(1Al). This indicates, in combination with the ^{27}Al MAS NMR spectra, that an increase of MSWI-FA leads to a general reduction of the PBG-matrix. Such an effect becomes even more apparent in PBG30 and PBG50.

The deconvolution of the ^{29}Si MAS spectra (Fig. 4) is performed assuming that the main contribution to the signal is due to silicon from MK, because of the abundance of the species in metakaolinite. The $Q^4_{Si}(0Al)/[Q^4_{Si}(3Al) + Q^4_{Si}(2Al)]$ ratio (0.57 in MK) steadily changes from 1.30, in PBG0, to 0.66, in PBG50. This hints at a progressive decrease in metakaolin dissolution.

3.4. Morphology observation

The microstructure of MSWI-FA, as revealed by SEM, is shown in Fig. S6. The morphological and mineralogical heterogeneity is proven by the occurrence of micrometric and sub-micrometric particles, of spherical, needle-like and more complex shapes, retaining features like an amorphous material. In Fig. 5, the micrographs of the internal surface of PBG0 and PBG30, recorded in secondary electron mode, are displayed. PBG0 appears compact, in agreement with its pervasive amorphous matrix. Some isolated fragments of unreacted MK (i.e., anatase, kaolinite, quartz) can be recognizable, along with micro-cracks. As expected, the EDS analyses revealed a composition rich in Al, Si and P. However, the two different amorphous systems, i.e., aluminophosphate and silica, are highly intermixed and not easily distinguishable from one another by SEM-EDS [9]. The matrix of PBG30 is similar to PBG0's, but more heterogeneous and with higher porosity. The composition of the matrix indicates an enrichment in alkali, i.e., Ca and Mg, confirming a degree of MSWI-FA particle dissolution, as discussed above. The increasing porosity is even more evident for PBG50 sample (Fig. 6), where relatively large pores favour the growth of acicular and needle-like Ca-phosphate crystals from the residual pore solution. In addition, the microstructure appears less dense, constituted of loosely bound particles rather than a condensed and compact matrix.

The cross section in backscattered mode of PBG30 (Fig. 7, top) shows Ca-phosphate evenly distributed in the PBG-matrix. Therefore, a 30 wt% of MK substituted with MSWI-FA allows an intermix of these two binding phases, leading to the cementation of the unreacted particles. Although the phosphate crystals and the unreacted MSWI-FA particles embedded in the PBG-matrix can potentially reinforce the resulting material, the increasing presence of pores, which act as stress concentrators, ultimately impairs the compressive strength (see next paragraph).

On the other hand, the PBG50 cross-section (Fig. 7, bottom) indicates a distribution of larger and more heterogenous particles, related to the increase of the MSWI-FA content and the reduced participation of MK to the final material. It is worth noticing how the P-map correlates with Ca and Mg's, while the distribution of Al is concentrated on the unreacted particles, indicating that in this case most of the binding action is due to Ca/Mg-phosphates.

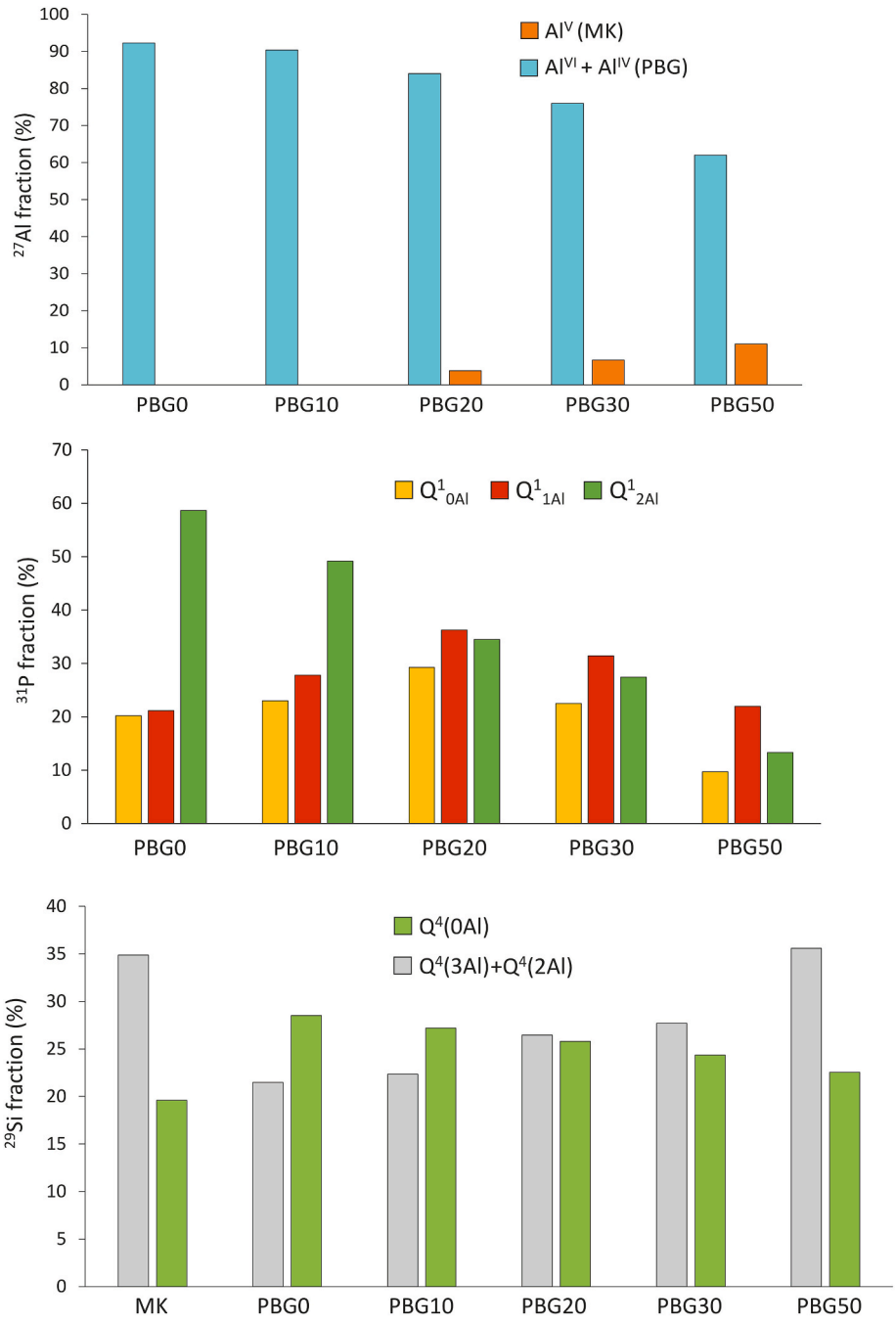

Fig. 4. ^{27}Al MAS (top), ^{31}P MAS (middle) and ^{29}Si MAS (bottom) deconvolution data of PBG samples cured for 60 days.

3.5. *Setting time, compressive strength and porosity*

The effects due to the setting time on the PBG samples are illustrated in Fig. 8 (top). PBG0 exhibits a final setting time of over 60 h, in agreement with the values reported in literature, which, in some cases can reach 18–20 day, as a function of the mix composition and curing mode [35]. Such behaviour is due to the slow kinetics of the deal-umination and polycondensation reactions [7]. Therefore, for practical purposes, in order to speed up the process, curing at comparatively high temperature (between 40 and 80 °C) is advisable [7,33]. Owing to the quick acid-base reactions involving the MSWI-FA alkali (Ca and Mg) with phosphate, the addition of MSWI-FA markedly shortens the setting time to a few hours or even less in the case of high substitution degrees. Such fast kinetics are reported for acid-base Mg phosphate and alkali-activated fly-ash-based binders [28,44]. Please, note that even PBG10, which is structurally and microstructurally similar to PBG0, displays a significant shortening of its setting time, of about 30%.

The compressive strength changes from early (7 days) to long-aging (60 days) of the PBG-samples are displayed in Fig. 8 (bottom). In all of the cases, the aging time positively affects the mechanical properties, testifying the strengthening effect of the geopolymerization and phosphate crystallization progress. The reference PBG0 reaches over 90% of the 60-day figure in the first week (i.e, 31.3 *versus* 34.6 MPa), suggesting that, at such conditions, the curing treatment of 24 h at 60 °C effectively speeds up the poly-condensation reactions towards their completion. A similar behaviour is revealed by PBG10, which displays close values of compressive strength between early and long-aging curings, 29.4 and 30.7 MPa, respectively. A significant change apparently takes place at higher MSWI-FA substitution degrees, with PBG20, PBG30 and PBG50 that exhibit 46%, 38% and 27% of the PBG0's strength from 60-days

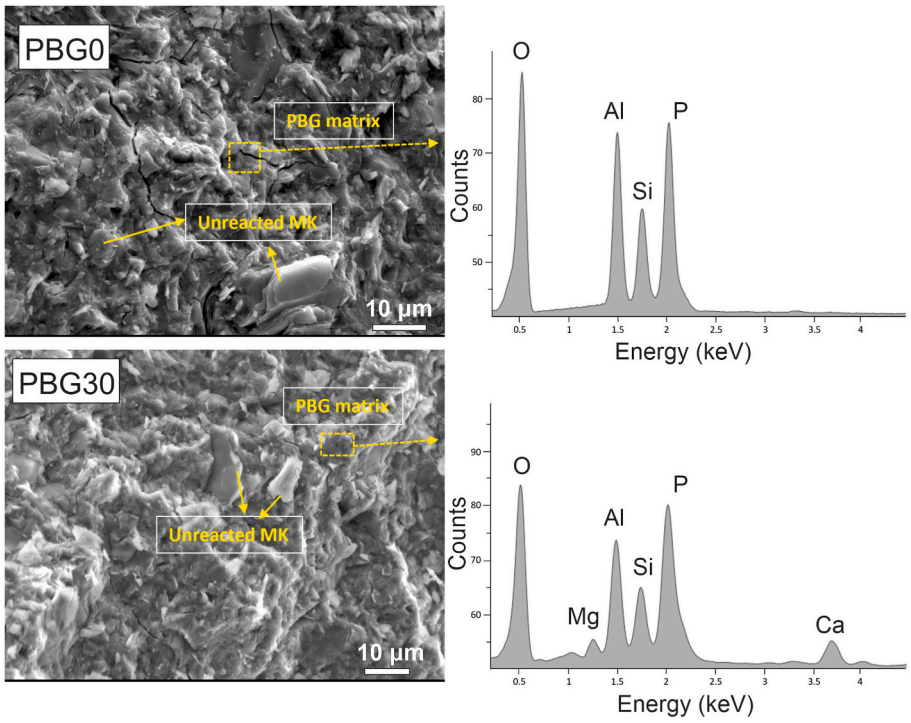

Fig. 5. SEM-EDS micrographs of PBG0 and PBG30 samples cured for 60 days.

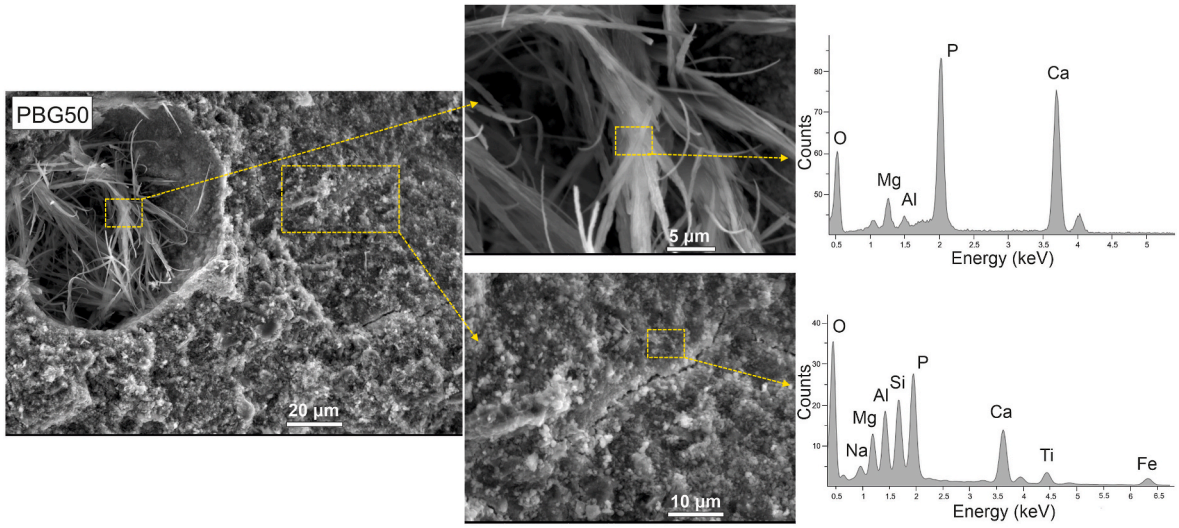

Fig. 6. SEM-EDS micrographs (bulk and pore's content) of PBG50 sample cured for 60 days.

curing. This is likely related to the gradual crystallization of Ca/Mg-phosphates from the acidic pore solution. Such a process contributes to build up a microstructure resembling that of a composite material with crystals embedded in an amorphous matrix (see Fig. 7, top). The development of such a microstructure, which reduces crack deflection and propagation [45], and induces a well-known toughening in ceramics [46,47] and in acid-base cements [48], is nevertheless accompanied by a significant increase in porosity, as proven by SEM observations. Therefore, the detrimental effect due to porosity seems to prevail over the expected improvement of the mechanical properties because of a composite-like microstructure, at MSWI-FA >10 wt%. The poorer performance of PBG20-30-50 than PBG10 is also ascribable to the abundance in the unreacted MSWI-FA fraction of low-strength phases (e.g. gypsum).

The total porosity measured by mercury intrusion is reported in Table 4. Given that the vacuum conditions required by measurements cause partial dehydration of the samples, the related results must be considered from a qualitative standpoint only. PBG0 exhibits low porosity (~1%), confirming the presence of a pervasive and compact aluminophosphate matrix. A similar value (3.5%) is observed for PBG10, while an increase to about 8% occurs in PBG20 and PBG30. The reduction of the paste setting time and fluidity in presence of MSWI-FA, along with the CO_2 production due to the dissolution of calcite, favour the development of a higher porosity, promoted by gas/air entrapment. This agrees with the high values of porosity observed in PBG50.

4. Discussion

The effects of the partial replacement of MK with of MSWI-FA in the phosphate-based geopolymer system can be explained by considering

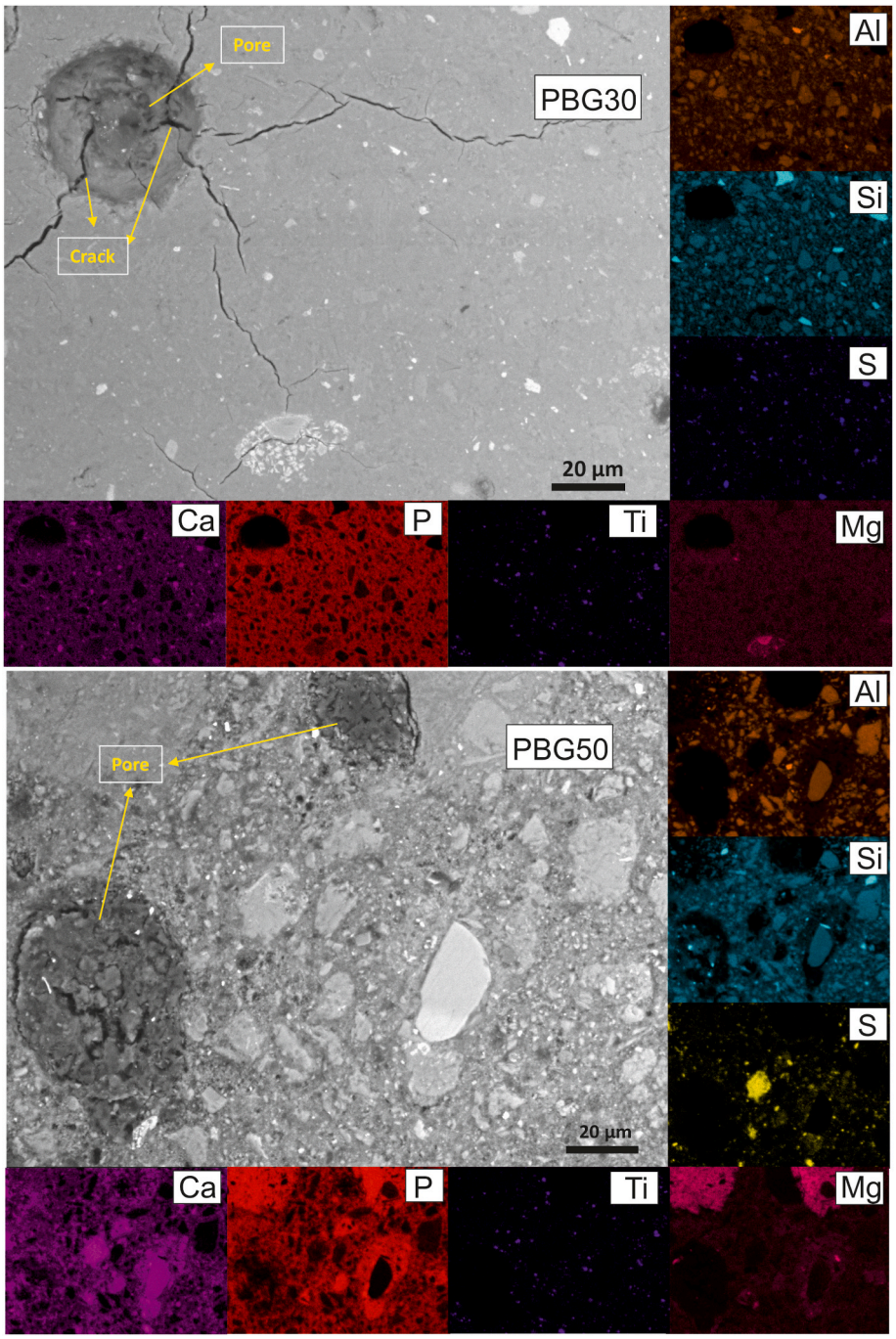

Fig. 7. Backscattered images of PBG30 and PBG50 cross-sections, with major elements' EDS maps.

the reaction conditions, the chemical/phase composition of the involved waste and the key parameters of the formulation (i.e., Al/P and L/S). In the PBG0 formulation, all of the available phosphate groups can potentially react with MK. Therefore, the highly acidic environment boosts MK depolymerization/dissolution, thus providing the building blocks necessary for the PBG condensation reactions, and eventually leading to the formation of Al-O-P linkages and amorphous SiO_2, as detected by SSNMR (section 3.3). The introduction of MSWI-FA causes a decrease of the overall content of Al_2O_3 in the mixture, because of the lower amount of alumina provided by MSWI-FA with respect to MK. The constraint of a fixed Al/P ratio reduces, as a consequence, the available phosphate partaking in the reactions. On the one hand, the liquid-to-solid ratio has to be increased to preserve an acceptable workability of the paste; on the other hand, MSWI-FA competes with MK for the available phosphate by precipitating Ca/Mg-phosphate hydrate phases. Such acid-base reactions are generally characterized by fast kinetics [29,48], all the more so here as favoured by the rapid dissolution of the MSWI-FA Ca/Mg-bearing amorphous and crystalline phases (i.e., calcite, periclase, ettringite; Table 4). By way of example, this explains the crystallization of brushite in PBG50, as observed by XRPD. Being a kinetically-driven process, precipitation occurs owing to a high Ca oversaturation and a relatively low brushite solubility product (Ksp = $10^{-6.5}$) [49], notwithstanding a Ca/P molar ratio lower than the theoretical one (0.83 instead of 1). A quick subtraction of both phosphate and water not only accelerates the paste hardening (Fig. 8), but also hinders the MK dealumination, as shown by ^{27}Al and ^{29}Si MAS spectra, although such acid-base reactions are highly exothermic and, hence, thermodynamically favoured [50,51]. As a net result, the availability of

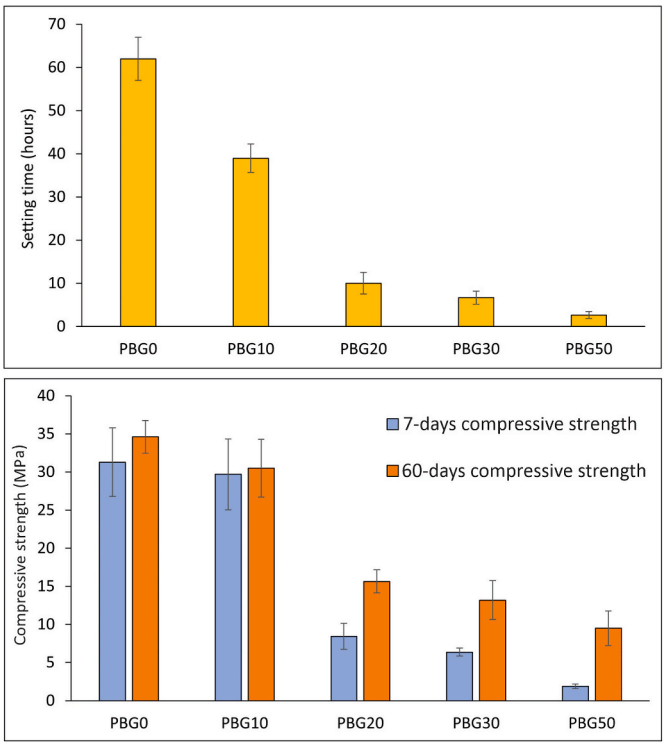

Fig. 8. Setting time (top) and early and long-aging compressive strength values (bottom) of PBG samples. Uncertainties determined as standard deviation of each measurement batch.

Table 4
Porosity measurements on PBG samples cured for 60 days. Standard deviation is around 15–20% of the average value.

Sample	Porosity (%)	Average pore size (nm)
PBG0	0.98	83.1
PBG10	3.80	42.3
PBG20	8.07	54.2
PBG30	7.57	26.6
PBG50	38.6	50.8

Al for the condensation reactions to build up the geopolymer framework is reduced. A fraction of Al from MSWI-FA participates in the formation of the PBG-matrix, but its contribution does not fully compensate for the replaced MK. All this is testified by the detailed ^{31}P MAS analysis in Fig. 4, which evidences that the reticulated Q^1_P(2Al) component significantly decreases with the MSWI-FA introduction.

Mechanical properties measured on long-aging samples and microstructural features correlate. In fact, low degrees of MK substitution with MSWI-FA (i.e., 10 wt%) modestly stymie the amount of the geopolymer matrix, so that the PBG0's mechanical performances are still preserved. At a higher content of MSWI-FA, the precipitation of secondary products (i.e. brushite and MCPM) and the indirect inhibiting effects on MK dealumination and geopolymer matrix generation result in a shift from a pure PBG-system to a progressively more porous CMPC/PBG composite-like system, which thing is detrimental to the mechanical performance (Fig. 9).

It is worth attention that, as shown in Fig. 7, PBG and $CaHPO_4$ exhibit an excellent intermixing, at least up to 30 wt% of substitution. The dilution effect due to the large gap in Al_2O_3 content between the two raw materials, along with the progressive increase of the internal porosity in the MSWI-FA bearing PBG-samples and the presence of low-strength phases in the ash residue (i.e. gypsum), contribute to worsen the mechanical properties of the output composite. Recent results about the

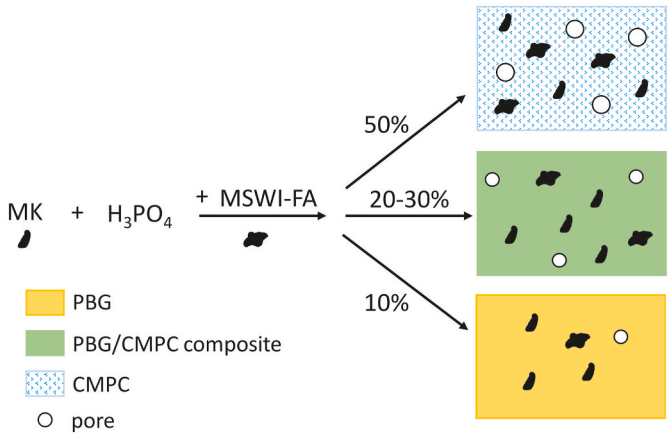

Fig. 9. Schematic representation of the influence of MSWI-FA degree of substitution in the production of PBG.

introduction of CFA in PBG indicated that the mechanical properties where not significantly affected up to 30% wt. MK substitution [17]. This can be explained with a better micro-aggregate and pore-filling effect of the CFA spherical particles with respect to the MK plate-like particles. On the other hand, Wang et al. showed that a 30% wt. substitution with low-calcium CFA (5.6% CaO) determined a 30% decrease of 28-days compressive strength, while the substitution with high-calcium CFA (16.5% Cao) lead to a 6.4% increase and a 15% decrease for a 20% wt. and 30% wt. substitution, respectively [18]. They argued that, in the first case, the LC-CFA lower reactivity with respect to MK caused a detrimental dilution effect, while the HC-CFA influence was probably related to a balance between the relative contribution of PBG and Ca-phosphate phases [18]. A similar mechanism could be at work in case of MSWI-FA, although the dilution effect is more relevant, because of the larger gap in Al_2O_3 content. Yet, the significant reduction of the final setting time promoted even by low MSWI-FA contents can potentially be of interest, as the long PBG reaction kinetics is one of the main drawbacks in terms of practical application [7,16], along with the relatively high cost of both MK and phosphoric acid. In this view, even a partial MK substitution with MSWI-FA can help mitigate technical problems and economic impact related to PBG use/production.

5. Conclusions

Water/steam-washed MSWI-FA has been introduced for the first time into phosphate-based geopolymer in partial replacement of metakaolin. Fractions of MSWI-FA participate in the reaction with the phosphoric acid, and amorphous phosphate hydrates form by exploiting metal ions, such as Mg^{2+}. The replacement of MK with MSWI-FA makes available Ca^{2+}, whose mobilization leads to the precipitation of crystalline Ca-phosphates. Yet, the lower amount of available aluminium provided by MSWI-FA in comparison with pure MK and the competition of the metal ions from ash for phosphates, hinder the development of the aluminophosphate geopolymer matrix. Using Al/P~1.1, at 10 wt% of MK substitution with MSWI-FA, the extent of geopolymerization is still satisfactory, in terms of relative contribution of P/Al-reticulation, as shown by Q^1_P(2Al) and octahedral [AlO_6] fractions, and the mechanical performance turns out to be comparable to the one exhibited by the reference sample, PBG0. At higher degrees of substitution (30–50 wt%), the nature of the resulting material gradually shifts from that of a PBG-system to a composite, obtained by an alkali-phosphate cement and PBG. Although a well-mixed microstructure is preserved up to 30 wt% substitution, the increasing porosity and the presence of low-strength phases lead to a decline of the mechanical performance at increasing MSWI-FA content.

Fundings

The present study (AP) has been partly funded by Ministero dell'Ambiente e della Tutela del Territorio e del Mare through the call: "CLEAN – Ceneri Leggere Eco-sostenibili per un Ambiente No-rifiuti" (m_amte.MiTE.REGISTRO UFFICIALE.USCITA.0049573.22-04-2022).

Declaration of competing interest

The authors declare that they have no known competing financial interests or personal relationships that could have appeared to influence the work reported in this paper.

Acknowledgments

A.V., L.Z., P.M. acknowledge support from the Czech Academy of Sciences, Institute of Theoretical and Applied Mechanics (RVO 68378297).

Appendix A. Supplementary data

Supplementary data to this article can be found online at https://doi.org/10.1016/j.ceramint.2023.04.042.

References

[1] L. Coppola, T. Bellezze, A. Belli, et al., Binders alternative to Portland cement and waste management for sustainable construction—part 1, J. Appl. Biomater. Funct. Mater. 16 (2018) 186–202, https://doi.org/10.1177/22808000187828.
[2] S.S. Hossain, P.K. Roy, Sustainable ceramics derived from solid wastes: a review, J. Asian Ceram. Soc. 8 (2020) 984–1009, https://doi.org/10.1080/21870764.2020.1815348.
[3] D.D. Del Rio, B.K. Sovacool, A.M. Foley, S. Griffiths, M. Bazilian, J. Kim, D. Rooney, Decarbonizing the ceramics industry: a systematic and critical review of policy options, developments and sociotechnical systems, Renewable Sustainable Energy Rev. 157 (2022), 112081, https://doi.org/10.1016/j.rser.2022.112081.
[4] F.B. da Costa, C.R. da Silva Morais, A.M. Rodrigues, Sustainable glass-ceramic foams manufactured from waste glass bottles and bentonite, Ceram. Int. 46 (11) (2020) 17957–17961, https://doi.org/10.1016/j.ceramint.2020.04.107.
[5] M.S. Masoule, N. Bahrami, M. Karimzadeh, B. Mohasanati, P. Shoaei, F. Ameri, T. Ozbakkaloglu, Lightweight geopolymer concrete: a critical review on the feasibility, mixture design, durability properties, and microstructure, Ceram. Int. 48 (8) (2022) 10347–10371, https://doi.org/10.1016/j.ceramint.2022.01.298.
[6] C. Bai, P. Colombo, Processing, properties and applications of highly porous geopolymers: a review, Ceram. Int. 44 (14) (2018) 16103–16118, https://doi.org/10.1016/j.ceramint.2018.05.219.
[7] Y.S. Wang, Y. Alrefaei, J.G. Dai, Silico - aluminophosphate and alkali-aluminosilicate geopolymers: a comparative review, Front. Mater. 6 (2019) 1–17, https://doi.org/10.3389/fmats.2019.00106.
[8] J. Davidovits, Geopolymers: ceramic-like inorganic polymers, J. Ceram. Sci. Technol. 8 (2017) 335–350, https://doi.org/10.4416/JCST2017-00038.
[9] J. Davidovits, Geopolymer Chemistry and Applications, fifth ed., Geopolymer Institute, 2020.
[10] P. Zhang, Z. Gao, J. Wang, J. Guo, S. Hu, Y. Ling, Properties of fresh and hardened fly ash/slag based geopolymer concrete: a review, J. Clean. Prod. 270 (2020), 122389, https://doi.org/10.1016/j.jclepro.2020.122389.
[11] S. Qaidi, H.M. Najm, S.M. Abed, H.U. Ahmed, H. Al Dughaishi, J. Al Lawati, M. M. Sabri, F. Alkhatib, A. Milad, Fly ash-based geopolymer composites: a review of the compressive strength and microstructure analysis, Materials 15 (2022) 7098, https://doi.org/10.3390/ma15207098.
[12] X. He, Z. Yuhua, S. Qaidi, H.F. Isleem, O. Zaid, F. Althoey, J. Ahmad, Mine tailings-based geopolymers: a comprehensive review, Ceram. Int. 48 (2022) 24192–24212, https://doi.org/10.1016/j.ceramint.2022.05.345.
[13] J. Liu, Z. Wang, G. Xie, Z. Li, X. Fan, W. Zhang, F. Xing, L. Tang, J. Ren, Resource utilization of municipal solid waste incineration fly ash - cement and alkali-activated cementitious materials: a review, Sci. Total Environ. 852 (2022), 158254, https://doi.org/10.1016/j.scitotenv.2022.158254.
[14] X. Zhan, L. Wang, L. Wang, X. Wang, J. Gong, L. Yang, J. Bai, Enhanced geopolymeric co-disposal efficiency of heavy metals from MSWI fly ash and electrolytic manganese residue using complex alkaline and calcining pre-treatment, Waste Manag. 98 (2019) 135–143, https://doi.org/10.1016/j.wasman.2019.08.024.
[15] A. Katsiki, Aluminosilicate phosphate cements–a critical review, Adv. Appl. Ceram. 118 (2019) 274–286, https://doi.org/10.1080/17436753.2019.1572339.
[16] S. Ma, Z. Zhang, X. Liu, Comprehensive understanding of aluminosilicate phosphate geopolymers: a critical review, Materials 15 (2022) 5961, https://doi.org/10.3390/ma15175961.
[17] H. Guo, P. Yuan, B. Zhang, Q. Wang, L. Deng, D. Liu, Realization of high-percentage addition of fly ash in the materials for the preparation of geopolymer derived from acid-activated metakaolin, J. Clean. Prod. 285 (2021), 125430, https://doi.org/10.1016/j.jclepro.2020.125430.
[18] Y.S. Wang, Y. Alrefaei, J.G. Dai, Influence of coal fly ash on the early performance enhancement and formation mechanisms of silico–aluminophosphate geopolymer, Cement Concr. Res. 127 (2020), 105932, https://doi.org/10.1016/j.cemconres.2019.105932.
[19] E. Destefanis, C. Caviglia, D. Bernasconi, E. Bicchi, R. Boero, C. Bonadiman, G. Confalonieri, I. Corazzari, G. Mandrone, L. Pastero, A. Pavese, F. Turci, Q. Wehrung, Valorization of mswi bottom ash as a function of particle size distribution, using steam washing, Sustainability 12 (2021) 1–17, https://doi.org/10.3390/su12229461.
[20] C. Caviglia, E. Destefanis, L. Pastero, D. Bernasconi, C. Bonadiman, A. Pavese, MSWI fly ash multiple washing: kinetics of dissolution in water, as function of time, temperature and dilution, Minerals 12 (2022) 742, https://doi.org/10.3390/min12060742.
[21] M. Ajorloo, M. Ghodrat, J. Scott, V. Strezov, Heavy metals removal/stabilization from municipal solid waste incineration fly ash: a review and recent trends, J. Mater. Cycles Waste Manag. 24 (2022) 1693–1717, https://doi.org/10.1007/s10163-022-01459-w.
[22] A. Ferraro, I. Farina, M. Race, F. Colangelo, R. Cioffi, M. Fabbricino, Pre-treatments of MSWI fly-ashes: a comprehensive review to determine optimal conditions for their reuse and/or environmentally sustainable disposal, Rev. Environ. Sci. Biotechnol. 18 (2019) 453–471, https://doi.org/10.1007/s11157-019-09504-1.
[23] C.H. Lam, A.W. Ip, J.P. Barford, G. McKay, Use of incineration MSW ash: a review, Sustainability 2 (2010) 1943–1968, https://doi.org/10.3390/su2071943.
[24] A.M. Joseph, R. Snellings, P. Van den Heede, S. Matthys, N. De Belie, The use of municipal solid waste incineration ash in various building materials: a Belgian point of view, Materials 11 (2018) 141, https://doi.org/10.3390/ma11010141.
[25] O. Ginés, J.M. Chimenos, A. Vizcarro, J. Formosa, J.R. Rosell, Combined use of MSWI bottom ash and fly ash as aggregate in concrete formulation: environmental and mechanical considerations, J. Hazard Mater. 169 (2009) 643–650, https://doi.org/10.1016/j.jhazmat.2009.03.141.
[26] B.H. Cho, B.H. Nam, J. An, H. Youn, Municipal solid waste incineration (MSWI) ashes as construction materials—a review, Materials 13 (2020) 3143, https://doi.org/10.3390/ma13143143.
[27] K. Yin, A. Ahamed, G. Lisak, Environmental perspectives of recycling various combustion ashes in cement production—a review, Waste Manag. 78 (2018) 401–416, https://doi.org/10.1016/j.wasman.2018.06.012.
[28] A. Viani, K. Sotiriadis, P. Šašek, M.S. Appavou, Evolution of microstructure and performance in magnesium potassium phosphate ceramics: role of sintering temperature of MgO powder, Ceram. Int. 42 (2016) 16310–16316, https://doi.org/10.1016/j.ceramint.2016.07.182.
[29] A.D. Wilson, J.W. Nicholson, Acid-base Cements. Their Biomedical and Industrial Applications, Cambridge University Press, Cambridge, 1993.
[30] D. Bernasconi, C. Caviglia, E. Destefanis, A. Agostino, R. Boero, N. Marinoni, C. Bonadiman, A. Pavese, Influence of speciation distribution and particle size on heavy metal leaching from MSWI fly ash, Waste Manag. 138 (2022) 318–327, https://doi.org/10.1016/j.wasman.2021.12.008.
[31] H. Lin, H. Liu, Y. Li, X. Kong, Properties and reaction mechanism of phosphoric acid activated metakaolin geopolymer at varied curing temperatures, Cement Concr. Res. 144 (2021), 106425, https://doi.org/10.1016/j.cemconres.2021.106425.
[32] H. Celerier, J. Jouin, N. Tessier-Doyen, S. Rossignol, Influence of various metakaolin raw materials on the water and fire resistance of geopolymers prepared in phosphoric acid, J. Non-Cryst. Solids 500 (2018) 493–501, https://doi.org/10.1016/j.jnoncrysol.2018.09.005.
[33] R.E. Damons, F.W. Petersen, An aspen model for the treatment of acid mine water, EJMP & EP 2 (2002) 69–81.
[34] A.P. Legrand, H. Sfihi, N. Lequeux, J. Lemaître, ^{31}P Solid-State NMR study of the chemical setting process of a dual-paste injectable brushite cements, J. Biomed. Mater. Res. 91B (2009) 46–54, https://doi.org/10.1002/jbm.b.31372.
[35] V. Mathivet, J. Jouin, A. Gharzouni, I. Sobrados, H. Celerier, S. Rossignol, M. Parlier, Acid-based geopolymers: understanding of the structural evolutions during consolidation and after thermal treatments, J. Non-Cryst. Solids 512 (2019) 90–97, https://doi.org/10.1016/j.jnoncrysol.2019.02.025.
[36] Y. Kim, M.C. Caumon, O. Barres, A. Sall, J. Cauzid, Identification and composition of carbonate minerals of the calcite structure by Raman and infrared spectroscopies using portable devices, Spectrochim. Acta A Mol. Biomol. 261 (2021), 119980, https://doi.org/10.1016/j.saa.2021.119980.
[37] F. Jones, Infrared investigation of barite and gypsumcrystallization: evidence for an amorphous to crystalline transition, CrystEngComm 14 (2012) 8374–8381, https://doi.org/10.1039/C2CE25918D.
[38] M. Zribi, S. Baklouti, Investigation of Phosphate based geopolymers formation mechanism, J. Non-Cryst. Solids 562 (2021), 120777, https://doi.org/10.1016/j.jnoncrysol.2021.120777.
[39] J. Sánchez-Enríquez, J. Reyes-Gasga, Obtaining $Ca(H_2PO_4)_2{\cdot}H_2O$, monocalcium phosphate monohydrate, via monetite from brushite by using sonication, Ultrason. Sonochem. 20 (2013) 948–954, https://doi.org/10.1016/j.ultsonch.2012.10.019.
[40] M. Edén, NMR studies of oxide-based glasses, Annu. Rep. Prog. Chem., Sect. C: Phys. Chem. 108 (2012) 177–221, https://doi.org/10.1039/C2PC90006H.
[41] T. Dong, S. Xie, J. Wang, Z. Chen, Q. Liu, Properties and characterization of a metakaolin phosphate acid–based geopolymer synthesized in a humid environment, J. Australas. Ceram. Soc. 56 (2020) 175–184, https://doi.org/10.1007/s41779-019-00376-w.

[42] S.N. Scrimgeour, J.A. Chudek, G.A. Cowper, C.H. Lloyd, ^{31})P solid-state MAS-NMR spectroscopy of the compounds that form in phosphate-bonded dental casting investment materials during setting, Dent. Mater. 23 (2007) 934–943, https://doi.org/10.1016/j.dental.2006.08.002.

[43] H. Celerier, J. Jouin, A. Gharzouni, V. Mathivet, I. Sobrados, N. Tessier-Doyen, S. Rossignol, Relation between working properties and structural properties from ^{27}Al, ^{29}Si and ^{31}P NMR and XRD of acid-based geopolymers from 25 to 1000°C, Mater. Chem. Phys. 228 (2019) 293–302, https://doi.org/10.1016/j.matchemphys.2019.02.049.

[44] W. Lee, J. Van Deventer, The effect of ionic contaminants on the early-age properties of alkali-activated fly ash-based cements, Cement Concr. Res. 32 (2002) 577–584, https://doi.org/10.1016/S0008-8846(01)00724-4.

[45] J. Mecholsky, Toughening in glass ceramic through microstructural design, in: R. C. Bradt, A.G. Evans, D. Hasselman, F.F. Lange (Eds.), Fracture Mechanics of Ceramics, vol. 6, Plenum Press, New York, NY, 1983.

[46] F.C. Serbena, I. Mathias, C.E. Foerster, E.D. Zanotto, Crystallization toughening of a model glass-ceramic, Acta Mater. 86 (2015) 216–228, https://doi.org/10.1016/j.actamat.2014.12.007.

[47] E. Apel, J. Deubener, A. Bernard, M. Holand, R. Muller, H. Kappert, Phenomena and mechanisms of crack propagation in glass-ceramics, J. Mech. Behav. Biomed. Mater. 1 (2008) 313–325, https://doi.org/10.1016/j.jmbbm.2007.11.005.

[48] A.S. Wagh, Chemically Bonded Phosphate Ceramics, second ed., Elsevier, 2016.

[49] L.C. Chow, Next generation calcium phosphate-based biomaterials, Dent. Mater. J. 28 (2009) 1–10, https://doi.org/10.4012/dmj.28.1.

[50] A. Viani, G. Lanzafame, D. Chateigner, Y. El Mendili, K. Sotiriadis, L. Mancini, M. Zucali, B. Ouladdiaf, Microstructural evolution and texture analysis of magnesium phosphate cement, J. Am. Ceram. Soc. 103 (2020) 1414–1424, https://doi.org/10.1111/jace.16782.

[51] P. Mácová, A. Viani, Investigation of setting reaction in magnesium potassium phosphate ceramics with time resolved infrared spectroscopy, Mater. Lett. 205 (2017) 62–66, https://doi.org/10.1016/j.matlet.2017.06.063.